

Damage and fracture of brittle materials subjected to tri-axial compression

A. LITEWKA⁽¹⁾, L. SZOJDA⁽²⁾

⁽¹⁾ *Universidade da Beira Interior,
Departamento de Engenharia Civil,
Covilhã, Portugal
e-mail: litewka@ubi.pt*

⁽²⁾ *Silesian University of Technology,
Department of Civil Engineering,
Gliwice, Poland*

THE AIM OF THE PAPER is to present the experimental and theoretical study of fracture of brittle materials. To this end, new and more complete experimental data on deformability and fracture of brick and mortar subjected to tri-axial state of stress were discussed. Such experimental data are necessary to formulate the theoretical models capable of describing the mechanical behaviour of concrete, cementitious composites, ceramics and rocks. The second objective of this study is to present the potentialities of our own phenomenological model, based on continuum damage mechanics and on the theory of tensor function representation. Comparison of the experimental results obtained for tri-axial compression of brick and mortar with respective theoretical predictions showed satisfactory agreement.

1. Introduction

THE PROGRESS IN MECHANICS of solids and structures requires mutually interrelated extensive theoretical and experimental studies of mechanical properties of structural materials, which are necessary to formulate theoretical models capable of describing the physical processes observed in solids subjected to multi-axial states of stress. Strong motivation for such experiments exists in the case of brittle rock-like materials because of complexity of the phenomena that affect their mechanical response. Some rather incomplete experimental data for rocks subjected to confined pressure presented by CRISTESCU and HUNSCHE [9], DERSKI *et al.* [10], GOODMAN [15] and RUMMEL [46] and similar but very limited results shown for concrete by CHEN [8] and NEVILLE [42], could give only preliminary information on the behaviour of brittle rock-like materials tested under tri-axial states of stress. Wide utilisation of ceramics and cementitious composites requires deeper studies of such phenomena like load or deformation-induced anisotropy that develops in the loading process due to internal oriented

damage growth. Simultaneously, new approaches based on micromechanics [1, 21, 23] and on the methods of continuum damage mechanics have been used by CHABOCHE *et al.* [7], LITEWKA *et al.* [31], MURAKAMI and KAMIYA [40] and HALM and DRAGON [16, 17] to formulate some phenomenological models capable of describing the mechanical behaviour of brittle rock-like materials in the presence of damage-induced anisotropy. Further developments and practical applications of these theoretical descriptions can be found in more recent papers [24, 34, 35]. However, those analyses are based on limited experimental data, particularly for tri-axial state of stress and were verified for some specific cases of loading only. To obtain more realistic theoretical description of overall material response, further extensive experimental studies are needed.

The aim of this note is to supply new and more complete experimental data on mechanical response of brittle materials subjected to tri-axial states of stress. To this end, a well known tri-axial test used mainly in rock mechanics [9, 10, 15] that consists in simultaneous action of axial compressive stress and hydrostatic pressure, referred to as a confining pressure, was employed. However, this classical procedure is not sufficient to obtain appropriate information on deformability, damage growth and fracture of brittle materials and that is why one more tri-axial test was used here to determine experimentally the behaviour of brick and mortar. The second objective of the study presented here is to show the potentialities of our own phenomenological model [31, 32, 34, 35], based on continuum damage mechanics [19, 22, 27, 39] and on the theory of tensor function representation [3, 4, 45, 47], that can be used to describe the response, of brittle rock-like material subjected to tri-axial state of stress.

2. Theoretical background

Theoretical and experimental studies by CHEN [8], HORII and NEMAT-NASSER [20], MITROFANOV and DOVZENKO [38] and BOGUCKA *et al.* [5] showed that compressive load applied to brittle rock-like materials results in development of oriented microcracks perpendicular to the direction of maximum principal stress. However, the mechanism of oriented damage growth strongly depends on the state of stress and the overall structural degradation of the material is different for tension, compression and for combination of both the cases. It means that an originally isotropic material becomes orthotropic, with principal axes of orthotropy coinciding with the directions of the principal stresses. Early attempts to describe the mechanical behaviour of brittle materials by using the methods of damage mechanics can be found in [11, 14]. According to the rules of the continuum damage mechanics, the current state of the deteriorated material structure can be described by a certain independent variable or a group of variables [43] responsible for the current state of the material structure. Mathe-

mathematical model of deformability of brittle rock-like materials used in this paper is based on the assumption of tensorial nature of the material damage [26]. That is why the symmetric second-rank damage tensor defined by VAKULENKO and KACHANOV [50], MURAKAMI and OHNO [41] and BETTEN [2] was used as a variable responsible for deterioration of the material internal structure. Explicit form of the relevant constitutive equations was found by employing the methods of the theory of tensor function representations, as applied to solid mechanics by BOEHLER [4] and BETTEN [3]. Some results of possible application of the above theory to describe a nonlinear behaviour of concrete, fibre concrete and rocks including the experimental verification was explained elsewhere [31, 33, 34, 35]. The constitutive equations presented there consist of the stress-strain relations for anisotropic elastic solids:

$$(2.1) \quad \varepsilon_{ij} = A_{ijkl}\sigma_{kl},$$

where ε_{ij} is the strain tensor and σ_{kl} is the stress tensor. The fourth-order tensor A_{ijkl} that appears in Eq. (2.1) is a function of the damage effect tensor D_{ij} explained in [29, 30] and defines the material constants of an orthotropically damaged solid. It was shown earlier [31, 35] that instead of the most general representation of such a tensor function the following linear form seems to be sufficient:

$$(2.2) \quad A_{ijkl} = -\frac{\nu_0}{E_0}\delta_{ij}\delta_{kl} + \frac{1+\nu_0}{2E_0}(\delta_{ik}\delta_{jl} + \delta_{il}\delta_{jk}) \\ + C(\delta_{ij}D_{kl} + D_{ij}\delta_{kl}) + D(\delta_{ik}D_{jl} + \delta_{jl}D_{ik} + \delta_{il}D_{jk} + \delta_{jk}D_{il}).$$

Equation (2.2) contains the Kronecker delta δ_{ij} , the Young modulus E_0 and Poisson's ratio ν_0 for an originally undamaged material, two constants C and D to be determined experimentally and the second-order symmetric damage effect tensor D_{ij} responsible for the current state of internal structure of the material. Substituting Eq. (2.2) to the stress-strain relation (2.1), the following tensor function was obtained:

$$(2.3) \quad \varepsilon_{ij} = -\frac{\nu_0}{E_0}\delta_{ij}\sigma_{kk} + \frac{1+\nu_0}{E_0}\sigma_{ij} \\ + C(\delta_{ij}D_{kl}\sigma_{kl} + D_{ij}\sigma_{kk}) + 2D(\sigma_{ik}D_{kj} + D_{ik}\sigma_{kj})$$

which describes the anisotropic elastic response of the damaged material.

Deterioration of the material structure due to applied load can be described by the damage evolution equation expressed in the form of the tensor function

$$(2.4) \quad \Omega_{ij} = f_1\delta_{ij} + f_2\sigma_{ij} + f_3\sigma_{ik}\sigma_{kj},$$

where Ω_{ij} is a classical second-order damage tensor formulated by VAKULENKO and KACHANOV [50], MURAKAMI and OHNO [41] and BETTEN [2]. Our experiments [5, 32, 33] performed for plain concrete and fibre concrete show that the process of the damage growth starts at the very beginning of the loading and no significant evidence of damage threshold was noticed. That is why it seems to be reasonable to look for the damage evolution equation in the specific form expressed by Eq. (2.4) where the damage tensor depends directly on the stresses applied. Equation (2.4) contains three multipliers f_1, f_2 and f_3 that are scalar-valued functions of the stress tensor invariants. To determine the explicit form of these multipliers, what is necessary to describe the behaviour of the material subjected to a tri-axial state of stress, the analysis of mathematical properties of Eq. (2.4) was performed. Preliminary experimental verification of possible shape of this equation, by employing the available experimental results for uni-axial and bi-axial compression for concrete and rocks, are shown in [31, 34, 35]. It was found there that the respective scalar functions contained in Eq. (2.4) should have the following form:

$$(2.5) \quad \begin{aligned} f_1 &= A s_{kl} s_{kl} (1 + H \det \sigma_{pq})^F, \\ f_2 &= B \sqrt{\sigma_{kl} \sigma_{kl}} (1 + H \det \sigma_{pq})^F, \\ f_3 &= 0, \end{aligned}$$

where s_{kl} is the stress deviator and A, B, F are unknown material parameters to be determined experimentally. The multiplier H is a certain function of the scalar invariants of the stress tensor that should satisfy some requirements explained in [35]. New more general data presented in this note showed that the form of the multiplier H obtained in [35] is not sufficient to describe the properties of the materials subjected to a tri-axial state of stress. That is why it was finally found that H should be expressed by the following function of the stress tensor invariants:

$$(2.6) \quad H = \frac{227}{200 |\det \sigma_{rs}| + |\sigma_{ll}^3|}.$$

Taking into account Eqs. (2.5) and (2.6), the damage evolution equation (2.4) can be written in the following form:

$$(2.7) \quad \begin{aligned} \Omega_{ij} &= A s_{kl} s_{kl} \left(1 + \frac{227 \det \sigma_{pq}}{200 |\det \sigma_{rs}| + |\sigma_{ll}^3|} \right)^F \delta_{ij} \\ &\quad + B \sqrt{\sigma_{kl} \sigma_{kl}} \left(1 + \frac{227 \det \sigma_{pq}}{200 |\det \sigma_{rs}| + |\sigma_{ll}^3|} \right)^F \sigma_{ij}. \end{aligned}$$

The first term of Eq. (2.7) represents the isotropic damage and the second one accounts for the oriented damage due to different effects of the stress tensor components.

The damage tensor Ω_{ij} is very useful to describe the continuity of the material only. As it was shown earlier by MURAKAMI and OHNO [41] and LITEWKA [29, 30], such a damage tensor is not sufficient to describe the strength and stiffness reduction of the damaged material, and that is why it was necessary to define a second-order damage effect tensor D_{ij} . The relation

$$(2.8) \quad D_i = \frac{\Omega_i}{1 - \Omega_i}, \quad i = 1, 2, 3$$

between the principal values Ω_1 , Ω_2 and Ω_3 of the damage tensor Ω_{ij} and the principal components D_1 , D_2 and D_3 of the damage effect tensor D_{ij} contained in Eqs. (2.2) and (2.3) was formulated in [29].

3. Experiments

Most of the available experimental data on the mechanical behaviour of brittle rock-like materials like those obtained by KUPFER [25], EHM and SCHNEIDER [13], THIENEL *et al.* [49] and LIGEZA [28], concern the concrete subjected to a plane state of stress. Such experiments performed on suitably shaped concrete plates required special technique of bi-axial loading as well as elaboration of appropriate experimental procedure. As was shown in [36], numerous technical problems are faced when testing brittle rock-like materials under tri-axial state of stress. That is why, rather limited amount of the respective experimental data on the mechanical behaviour of materials subjected to such a state of stress can be found in the literature. The available experimental results concern mainly the rocks subjected to simultaneous action of axial compressive load represented by compressive stress σ_V and by hydrostatic pressure p , referred to as a confining pressure. This specific case of tri-axial loading shown in Fig. 1a corresponds to the state of stress observed in rocks and soils in natural deposits and that is why it is frequently used to study the properties of such materials. The data obtained from these experiments for some rocks and very scarce similar results available for concrete reported by CHEN [8] and NEVILLE [42], give some information on the behaviour of brittle rock-like materials and make it possible to conclude that the confining pressure increases the axial load that can be sustained. Moreover, in the limiting case when hydrostatic pressure only is applied, practically linear mechanical response of a material described by the law of elastic change of volume has been observed (CARVALHO *et al.* [6]).

To obtain more complete information on deformability, oriented damage growth and fracture for ceramics, concrete, cementitious composites and rocks,

further experimental studies are needed. That is why the classical procedure of tri-axial loading shown in Fig. 1a was extended by one more tri-axial test of simultaneous action of hydrostatic pressure and bi-axial uniform compression, explained in Fig. 1b. The experimental results presented here were obtained for cylindrical specimens of mortar and brick. The height and diameter of these specimens were equal to 12 cm and 6 cm, respectively. The program of loading consisted of uni-axial compression and two cases of tri-axial loading referred to as State I and State II as shown in Figure 1. Further details on the experimental technique adopted and the equipment used can be found elsewhere [36, 37, 48].

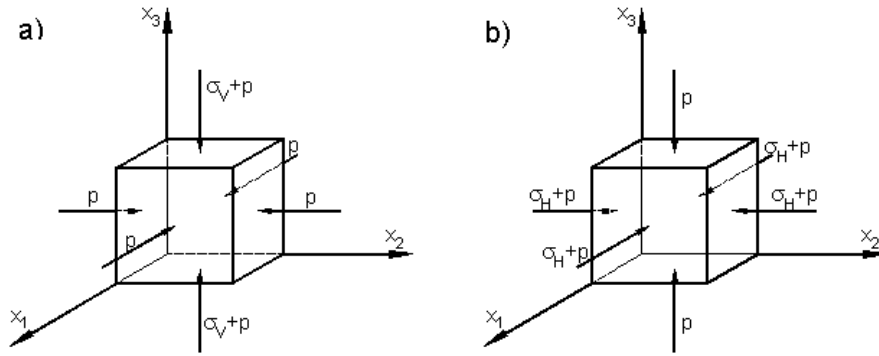


FIG. 1. Configuration of the stress tensor components for two cases of tri-axial state of stress: a) State I, b) State II.

The objective of the test performed under uni-axial compression was to calibrate the materials tested. That is why the initial Young modulus E_0 and Poisson's ratio ν_0 as well as the uni-axial compressive strength f_c shown in Table 1 were measured experimentally for both the materials tested. These values of standard constants as well as those for five other parameters A, B, C, D and F contained in Eqs. (2.2), (2.3), (2.5) and (2.7) are necessary to employ the theoretical model proposed. The various methods used to identify the four above constants, namely A, B, C and D , were presented in earlier papers [31, 32, 35]. Those methods are based on relevant experimental data for uni-axial or bi-axial compression of the material tested and the final form of the equations used to calculate these constants and other details related to the numerical procedure can be found in [32, 35]. The numerical values of the constants A, B, C and D shown in Table 1 were obtained by using the specific method of identification described in [35]. The comparison of experimental stress-strain curves determined for three specimens of brick and for four specimens of mortar, subjected to uni-axial compression with theoretical predictions obtained from Eqs. (2.3), (2.7) and (2.8), is shown in Figs. 2 and 3.

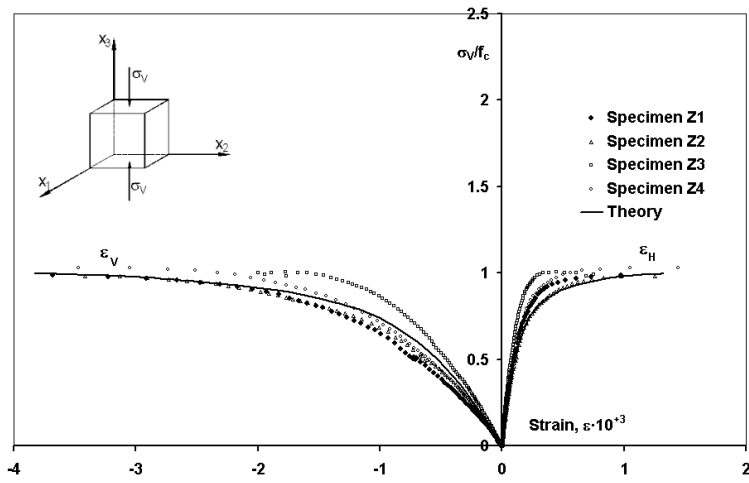


FIG. 2. Experimental and theoretical stress-strain curves for mortar subjected to uni-axial compression.

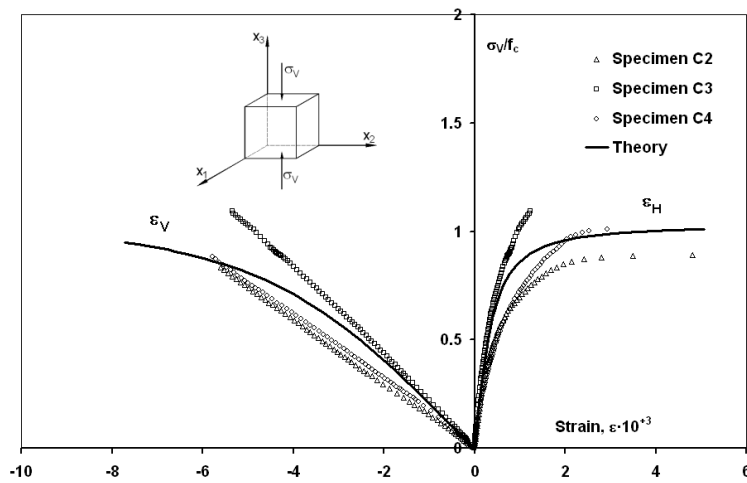


FIG. 3. Experimental and theoretical stress-strain curves for brick subjected to uni-axial compression.

The objective of the tests under tri-axial state of stress was to determine the respective stress-strain curves and to measure the stresses at material fracture for the prescribed loading programs. Various combinations of the stress tensor components and at least two different loading paths are necessary to supply the information on the shape of the limit surface at material failure subjected to tri-axial states of stress. The possible form of such a limit surface, together with

Table 1. Experimental data and constants used in the analysis of tri-axial state of stress of mortar and brick.

Constant	Unit	Mortar	Brick
E_0	MPa	8030	2420
ν_0	–	0.175	0.105
f_c	MPa	–7.39	–11.49
A	MPa^{-2}	2500×10^{-5}	1064×10^{-5}
B	MPa^{-2}	100.0×10^{-5}	100.0×10^{-5}
C	MPa^{-1}	-1.000×10^{-5}	-1.500×10^{-5}
D	MPa^{-1}	2.188×10^{-5}	3.508×10^{-5}
F	–	0.9400	0.6300

the loading paths for State I and State II of tri-axial compression is shown in Fig. 4. It is seen from this figure that respective loading paths consisted of two stages. The Stage 1 was the same in both cases of tri-axial loading and consisted in a monotonic increase of hydrostatic pressure up to the prescribed value p . In the Stage 2 of the first tri-axial state of stress (State I), the vertical normal stress σ_V was increased up to the material failure that occurs for $\sigma_{3f} = p + \sigma_V$. In the Stage 2 of the State II of tri-axial loading, two horizontal components σ_H of

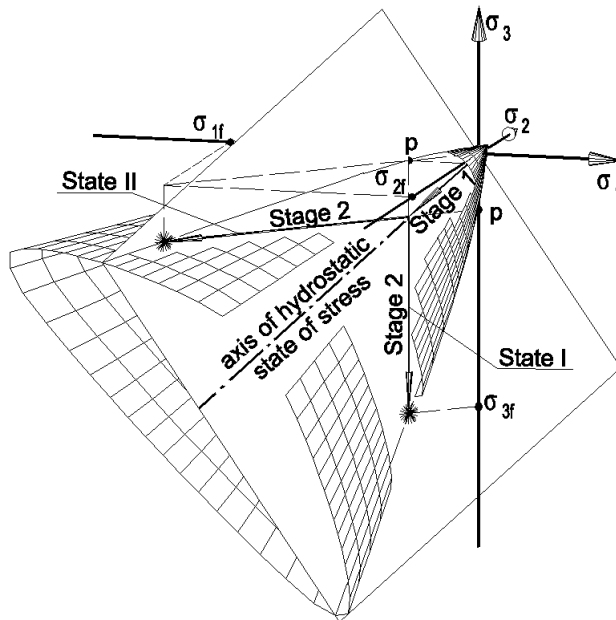


FIG. 4. Limit surface at material fracture and loading paths for State I and State II:
* point corresponding to material fracture.

uniform bi-axial state of stress were increased simultaneously up to the material failure that corresponds to $\sigma_{1f} = \sigma_{2f} = p + \sigma_H$. The experiments presented here have been performed for 6 specimens of brick and 6 specimens of mortar subjected to State I and for the same numbers of the specimens subjected to State II of the tri-axial compression. To obtain several combinations of the stress tensor components, various levels of the hydrostatic pressure p were used. The respective numerical data are shown in Tables 2 and 3.

Table 2. Magnitude of hydrostatic pressure p applied to brick and mortar in State I of tri-axial loading.

Material	Brick					
Specimen	CC1	CD1	CC2	CD2	CC3	CD3
Hydrostatic pressure p , MPa	-1.03	-1.03	-2.05	-2.05	-3.05	-3.05
Material	Mortar					
Specimen	ZC1	ZD1	ZC2	ZD2	ZC3	ZD3
Hydrostatic pressure p , MPa	-1.05	-1.05	-2.05	-2.05	-3.05	-3.05

Table 3. Magnitude of hydrostatic pressure p applied to brick and mortar in State II of tri-axial loading.

Material	Brick					
Specimen	CA1	CB1	CA2	CB2	CA3	CB3
Hydrostatic pressure p , MPa	0	0	-2.50	-2.50	-3.29	-3.54
Material	Mortar					
Specimen	ZA1	ZB1	ZA2	ZB2	ZA3	ZB3
Hydrostatic pressure p , MPa	0	-0.15	-1.95	-1.95	-3.62	-3.62

4. Stress-strain curves

Deformation of the specimen subjected to tri-axial loading should be determined at each stage of the loading process to supply the information necessary to construct the stress-strain curves for the material tested. That is why four electrical resistance strain gauges arranged in the form of two rosettes glued on opposite sides of the specimen were used to measure longitudinal and lateral deformations of the specimen. Unfortunately, these strain gauges were subjected to direct action of hydrostatic pressure applied to the lateral surface of the specimen and this unknown contribution of the hydrostatic pressure should be eliminated by using appropriate method of compensation. The details of the procedure of indirect compensation used in these experiments were presented in [36].

The stress-strain curves obtained experimentally for mortar and brick were compared with the theoretical predictions. To this end, the respective equations of the mathematical model used were expressed in terms of the stress tensor components

$$(4.1) \quad \sigma_{ij} = \begin{bmatrix} \sigma_{11} = p & 0 & 0 \\ 0 & \sigma_{22} = p & 0 \\ 0 & 0 & \sigma_{33} = \sigma_V + p \end{bmatrix}$$

for State I and

$$(4.2) \quad \sigma_{ij} = \begin{bmatrix} \sigma_{11} = \sigma_H + p & 0 & 0 \\ 0 & \sigma_{22} = \sigma_H + p & 0 \\ 0 & 0 & \sigma_{33} = p \end{bmatrix}$$

for State II. The stress-strain relation (2.3) specified for the stress tensors (4.1) and (4.2) have a form

$$(4.3) \quad \varepsilon_1 = \varepsilon_2 = -\frac{\nu_0}{E_0}\sigma_V + \frac{1-2\nu_0}{E_0}p + C[(D_1 + D_3)\sigma_V + p(5D_1 + D_3)] + 4DpD_1,$$

$$(4.4) \quad \varepsilon_3 = \frac{\sigma_V}{E_0} + \frac{1-2\nu_0}{E_0}p + C[2D_3\sigma_V + p(2D_1 + 4D_3)] + 4D(\sigma_V + p)D_3$$

for State I and

$$(4.5) \quad \varepsilon_1 = \varepsilon_2 = \frac{1-\nu_0}{E_0}\sigma_H + \frac{1-2\nu_0}{E_0}p + C[4D_1\sigma_H + p(5D_1 + D_3)] + 4D(\sigma_H + p)D_1,$$

$$(4.6) \quad \varepsilon_3 = -\frac{2\nu_0}{E_0}\sigma_H + \frac{1-2\nu_0}{E_0}p + C[2(D_1 + D_3)\sigma_H + p(2D_1 + 4D_3)] + 4DpD_3$$

for State II. Substituting the stress tensor components (4.1) and (4.2) to the damage evolution equation (2.7), one can obtain the following relations:

$$(4.7) \quad \Omega_1 = \Omega_2 = \left(\frac{2}{3}A\sigma_V^2 + Bp\sqrt{\sigma_V^2 + 2\sigma_V p + 3p^2} \right) \cdot \left[1 + \frac{227(\sigma_V + p)p^2}{200|(\sigma_V + p)p^2| + |(\sigma_V + 3p)^3|} \right]^F,$$

$$(4.8) \quad \Omega_3 = \left(\frac{2}{3} A \sigma_V^2 + B (\sigma_V + p) \sqrt{\sigma_V^2 + 2\sigma_V p + 3p^2} \right) \cdot \left[1 + \frac{227 (\sigma_V + p) p^2}{200 |(\sigma_V + p) p^2| + |(\sigma_V + 3p)^3|} \right]^F$$

for State I and

$$(4.9) \quad \Omega_1 = \Omega_2 = \left(\frac{2}{3} A \sigma_H^2 + B (\sigma_H + p) \sqrt{2\sigma_H^2 + 4\sigma_H p + 3p^2} \right) \cdot \left[1 + \frac{227 (\sigma_H + p)^2 p}{200 |(\sigma_H + p)^2 p| + |(2\sigma_H + 3p)^3|} \right]^F,$$

$$(4.10) \quad \Omega_3 = \left(\frac{2}{3} A \sigma_H^2 + B p \sqrt{2\sigma_H^2 + 4\sigma_H p + 3p^2} \right) \cdot \left[1 + \frac{227 (\sigma_H + p)^2 p}{200 |(\sigma_H + p)^2 p| + |(2\sigma_H + 3p)^3|} \right]^F$$

for State II. Equations (4.3)–(4.10) together with Eq. (2.8) make it possible to construct the theoretical stress-strain curves for mortar and brick. Comparison of these theoretical predictions with the corresponding experimental results is shown in Fig. 5, 6, 7, 8, 9, 10 and 11. It should be noted that theoretical curves were obtained for six material constants E_0 , ν_0 , A , B , C and D shown in Table 1 determined from uni-axial compression. The last constant F was determined by employing one experimental point for each material tested at a tri-axial compression.

The respective curves seen in Figs. 5–11 present the relation between the variable vertical component σ_V in State I or variable horizontal component σ_H for State II and the horizontal or vertical strains determined from the relations

$$\varepsilon_H = \varepsilon_1 - \frac{1 - 2\nu_0}{E_0} p,$$

$$\varepsilon_V = \varepsilon_3 - \frac{1 - 2\nu_0}{E_0} p,$$

where $\varepsilon_1 = \varepsilon_2$ and ε_3 are the principal strains measured experimentally for the specimens tested or determined theoretically from Eqs. (4.3)–(4.6).

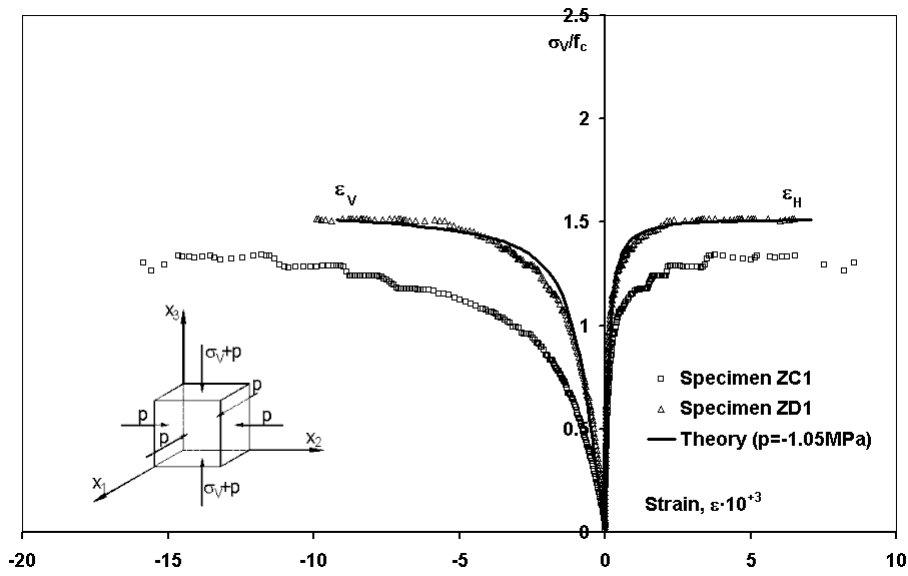


FIG. 5. Experimental and theoretical stress-strain curves for tri-axial compression (State I for $p = -1.05$ MPa) of mortar.

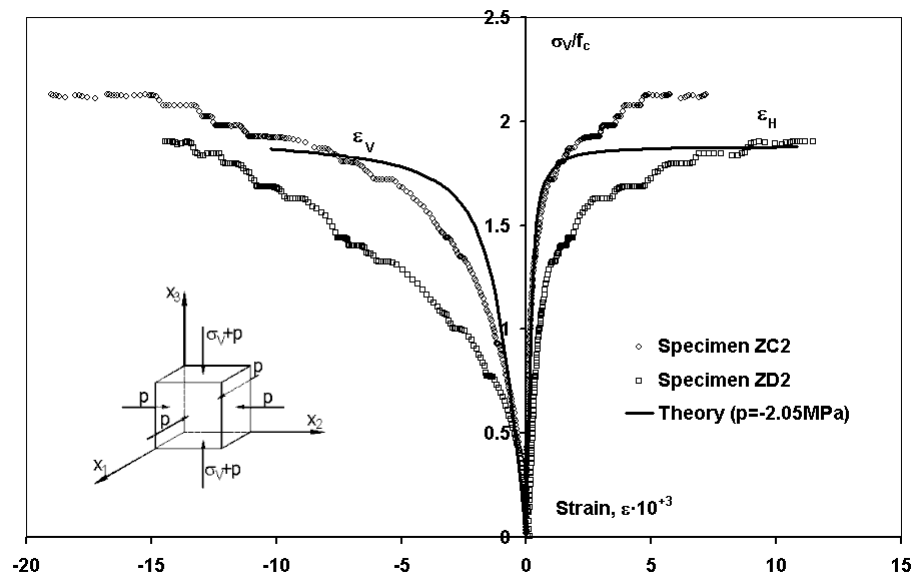


FIG. 6. Experimental and theoretical stress-strain curves for tri-axial compression (State I for $p = -2.05$ MPa) of mortar.

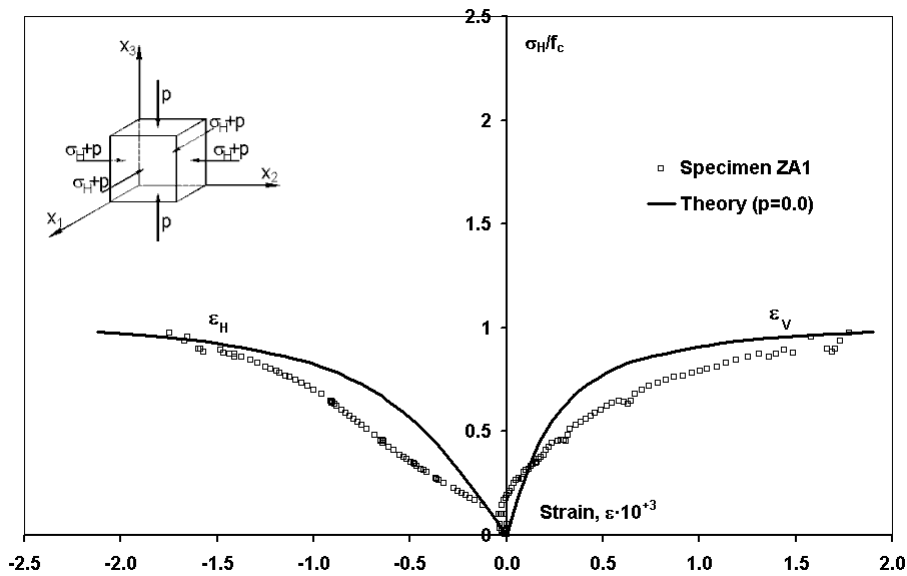


FIG. 7. Experimental and theoretical stress-strain curves for uniform bi-axial compression (State II for $p = 0$ MPa) of mortar.

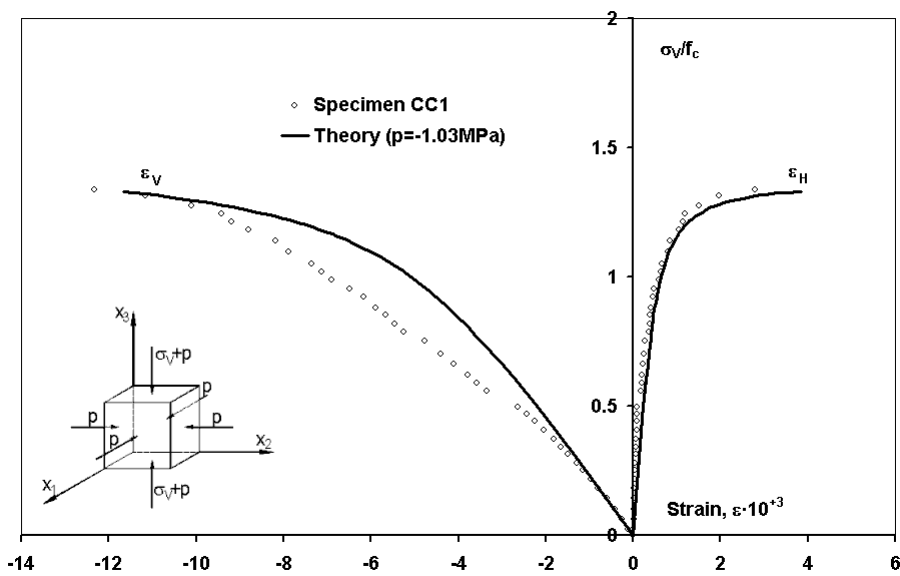


FIG. 8. Experimental and theoretical stress-strain curves for tri-axial compression (State I for $p = -1.03$ MPa) of brick.

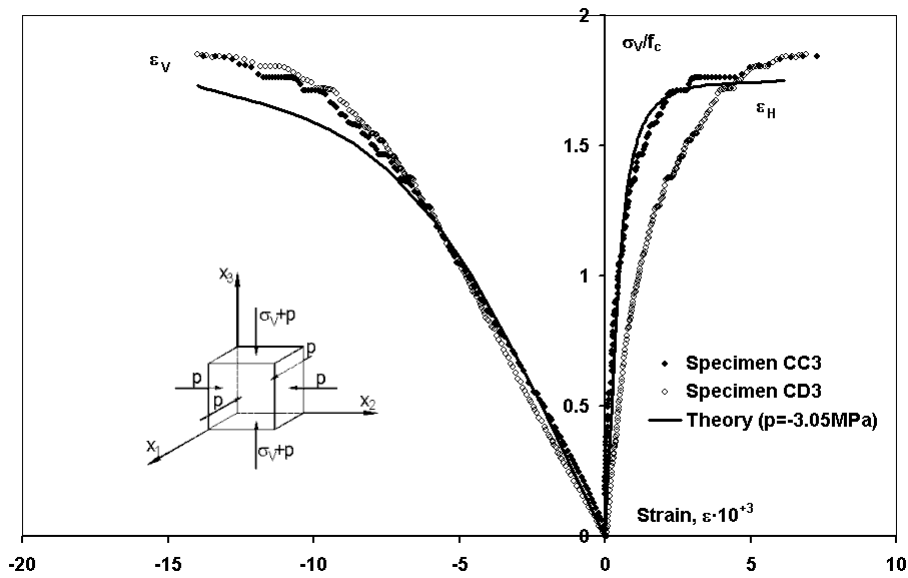


FIG. 9. Experimental and theoretical stress-strain curves for tri-axial compression (State I for $p = -3.05$ MPa) of brick.

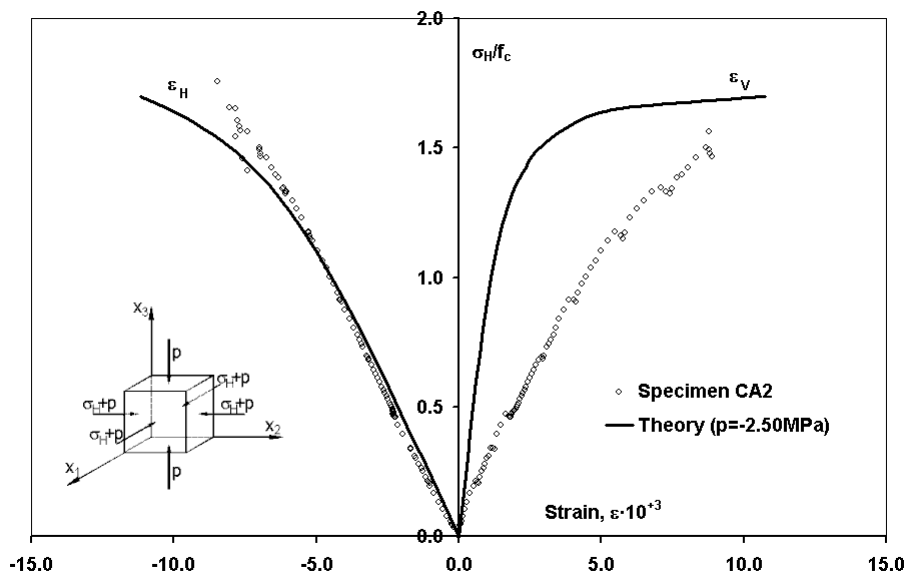


FIG. 10. Experimental and theoretical stress-strain curves for tri-axial compression (State II for $p = -2.50$ MPa) of brick.

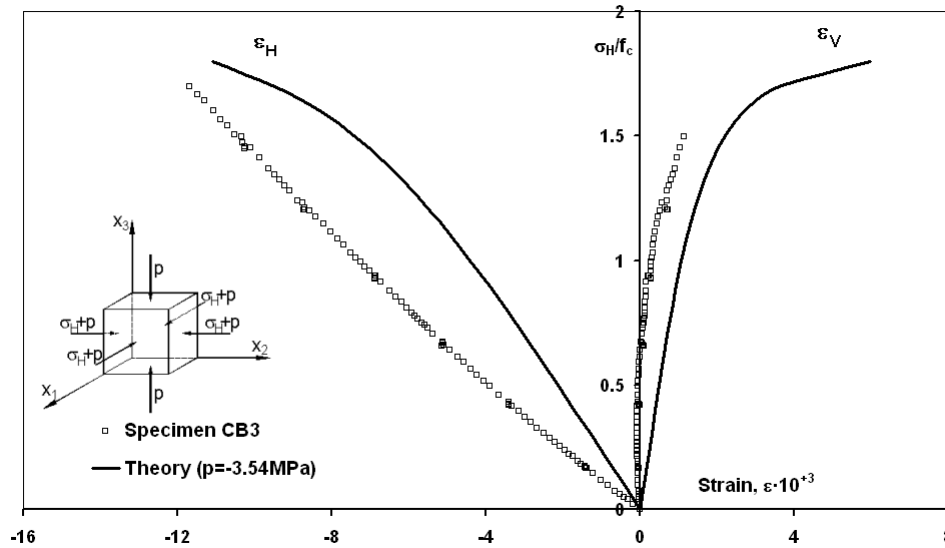


FIG. 11. Experimental and theoretical stress-strain curves for tri-axial compression (State II for $p = -3.49$ MPa) of brick.

5. Criterion of fracture

The theoretical model presented in this paper can also be used to determine the maximum stresses that can be sustained by the material subjected to multi-axial state of stress. To this end the appropriate criterion of material fracture should be formulated according to the rules of the damage mechanics. In the early stage of development of damage mechanics it was assumed that the material fracture occurs when scalar damage variable reaches its limiting value equal to unity. However, experimental observations presented by LEMAITRE [27], DYSON and MCLEAN [12], and HAYHURST [18] show that rupture of metals subjected to creep at elevated temperature occurs when the value of scalar damage parameter does not reach its limiting value equal to unity. This specific value of damage variable at material fracture referred to as a critical value of the scalar damage parameter [44] depends on the material, temperature and the state of stress applied and varies from 0.2 to 0.8. That is why the fracture criteria for metals subjected to damage are usually derived by employing the notion of such a critical value of the scalar damage parameter or critical configuration of the damage tensor components when the tensorial measure of damage is employed. The introduction of such a notion of critical state of material damage implies that in general case of the multi-axial state of stress, the material fracture begins when

the actual deteriorated internal structure, described by certain critical configuration of the damage tensor components, cannot sustain the load applied. Such an approach to the problem proved to be useful when formulating the respective rupture criteria for metals subjected to creep damage at elevated temperature [30] and probably may be necessary when dealing with uni-axial and bi-axial tension and compression of brittle rock-like materials.

The experiments presented in this paper show that the fracture mechanism of damaged brittle rock-like materials is different from that well known for metals subjected to damage. The examination of the specimens performed after fracture showed that the material tested was totally crushed into separate tiny particles. It means that tri-axial compression of brittle rock-like materials results in crack growth to such a state that at fracture, the net cross-section area is reduced to zero. This full deterioration of internal structure of the material occurs when at least one of the principal components Ω_1 , Ω_2 or Ω_3 of the damage tensor Ω_{ij} determined from Eq. (2.7) reaches the limiting value equal to unity. In such a case the material loses its continuity and its stiffness described by Eq. (2.2) decreases to zero, what results in a practically horizontal part of the theoretical stress-strain curves determined from Eq. (2.3) and shown in Fig. 5, 6, 7, 8 and 9. Lack of a pronounced horizontal part of the stress-strain curves for brick shown in Fig. 10 and 11 is a result of partial debonding of the electrical strain gauges at the advanced stage of deterioration of the material structure due to tri-axial loading.

To analyse the experimental results obtained for the two cases of tri-axial compression referred to as State I and State II Eq. (2.7) was expressed in terms of the stress tensors components shown in Eqs. (4.1) and (4.2). This substitution leads to Eqs. (4.7) and (4.8) for State I, and to Eqs. (4.9) and (4.10) for State II. The fracture of the material subjected to State I occurs when two horizontal principal components of the damage tensor Ω_1 and Ω_2 are equal to unity. It means that the fracture criterion in this case can be written in the form

$$(5.1) \quad \Omega_1 = \Omega_2 = \left(\frac{2}{3} A \sigma_V^2 + B p \sqrt{\sigma_V^2 + 2 \sigma_V p + 3 p^2} \right) \cdot \left[1 + \frac{227 (\sigma_V + p) p^2}{200 |(\sigma_V + p) p^2| + |(\sigma_V + 3p)^3|} \right]^F = 1.$$

The third principal component of the damage tensor Ω_3 does not decide in this case on the material fracture, since it grows slower than those determined by Eq. (5.1). The State II of tri-axial compression is characterised by faster growth

of the vertical principal component of the damage tensor Ω_3 and that is why the material fracture occurs when

$$(5.2) \quad \Omega_3 = \left(\frac{2}{3} A \sigma_H^2 + B p \sqrt{2\sigma_H^2 + 4\sigma_H p + 3p^2} \right) \cdot \left[1 + \frac{227 (\sigma_H + p)^2 p}{200 \left| (\sigma_H + p)^2 p \right| + \left| (2\sigma_H + 3p)^3 \right|} \right]^F = 1.$$

In this case the growth of two other principal components Ω_1 and Ω_2 of the damage tensor is slower and that is why they do not decide on the onset of fracture.

Equations (5.1) and (5.2) were used to determine the theoretical values of the stresses at material fracture

$$(5.3) \quad \sigma_{3f} = p + \sigma_V$$

for State I and

$$(5.4) \quad \sigma_{1f} = \sigma_{2f} = p + \sigma_H$$

for State II. Comparison of the theoretical predictions obtained from Eqs. (5.1)–(5.4) with the corresponding experimental data for mortar and brick is shown in Figs. 12, 13, 14 and 15. The maximum difference between the theoretical and

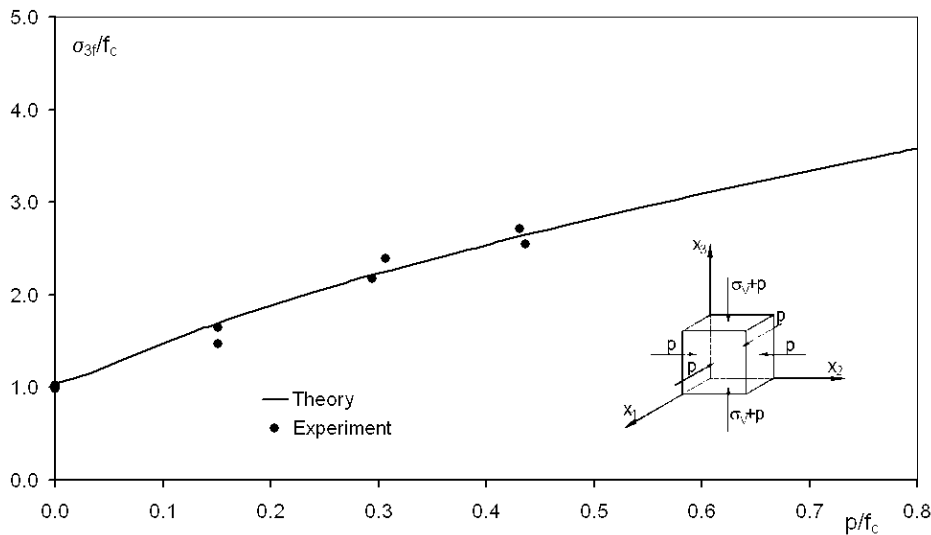


FIG. 12. Comparison of experimentally determined stresses at material fracture σ_{3f} with theoretical predictions for tri-axial State I of mortar.

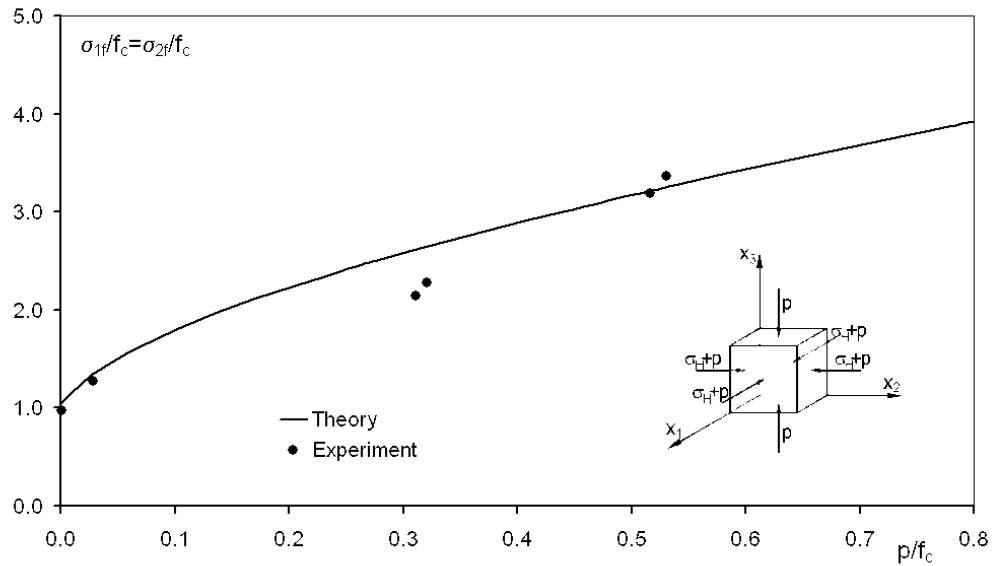


FIG. 13. Comparison of experimentally determined stresses at material fracture $\sigma_{1f} = \sigma_{2f}$ with theoretical predictions for tri-axial State II of mortar.

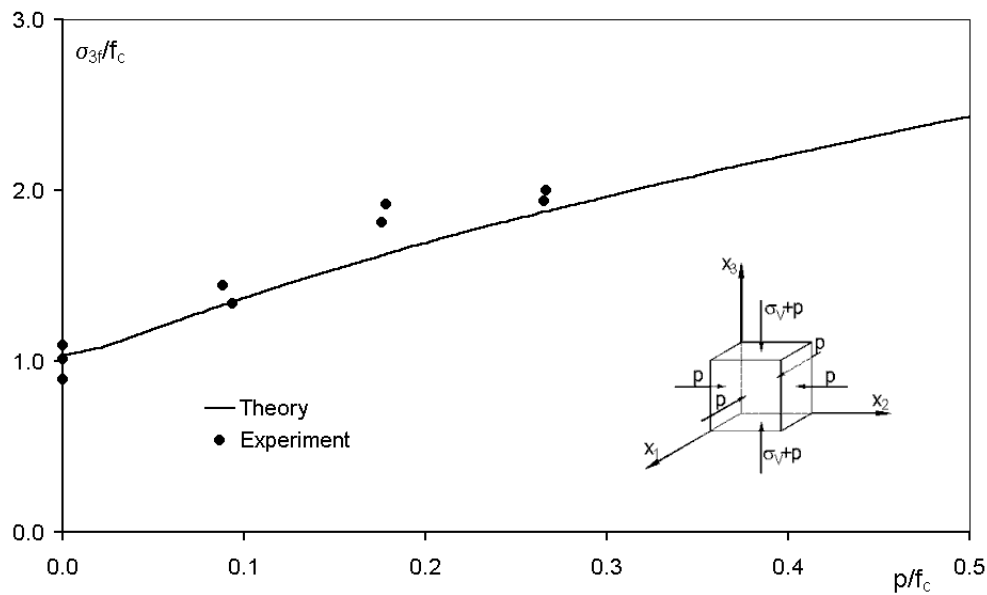


FIG. 14. Comparison of experimentally determined stresses at material fracture σ_{3f} with theoretical predictions for tri-axial State I of brick.

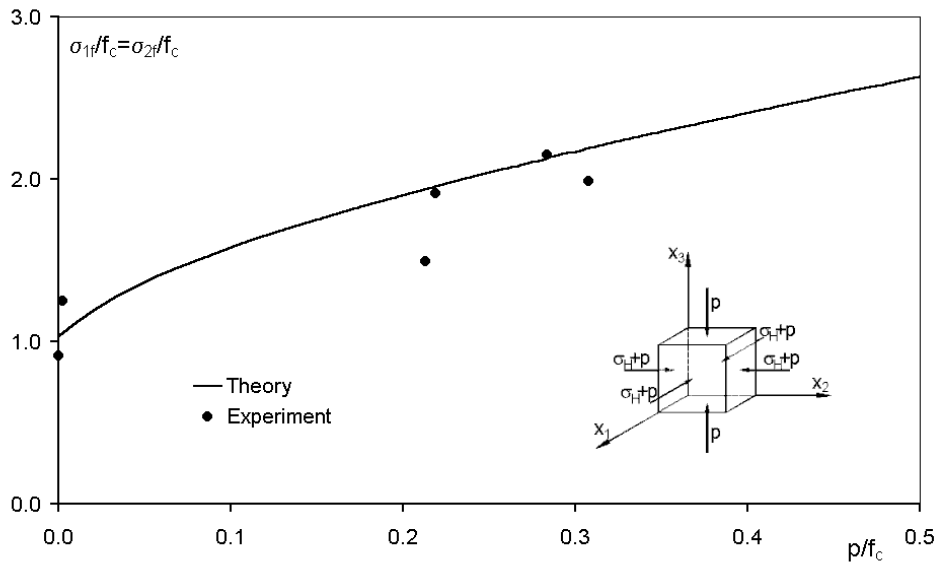


FIG. 15. Comparison of experimentally determined stresses at material fracture $\sigma_{1f} = \sigma_{2f}$ with theoretical predictions for tri-axial State II of brick.

experimental results seen in these figures for some specimens is approximately equal to 20%. The discrepancies obtained for other specimens are much smaller and the average difference determined for all the specimens tested does not exceed 0.3%. This relatively good agreement shows that overall accuracy of the theoretical model used in this paper is satisfactory.

6. Conclusions

Classical tri-axial test of confined axial compression used in rock mechanics is not sufficient to study the mechanical behaviour of brittle materials subjected to multi-axial state of stress. To obtain more complete information on the material response, at least two different tri-axial tests are necessary. That is why one more test of simultaneous action of uniform bi-axial compression and hydrostatic pressure was employed.

Theoretical model used here made it possible to describe the experimentally determined mechanical properties of mortar and brick. It was found that theoretical stress-strain curves for tri-axial loading obtained from the relevant equations show a satisfactory agreement with the experimental data. Fairly good agreement of the experimental data and theoretical predictions was also obtained for the stresses at the material fracture. Increasing compressive strength of brittle

rock-like materials known from earlier experiments for specimens subjected to confined axial compression was also observed in the new tri-axial test used here. This phenomenon can be explained theoretically within the mathematical model proposed. Thus, the experimental technique adopted and the phenomenological model used in this paper proved to be accurate enough to study the phenomena observed in tri-axial loading of brittle rock-like materials.

The mathematical model presented in this paper has a form necessary to describe our own as well as the other currently known and available experimental data for brittle rock-like materials that are limited to multi-axial but monotonic loading. Possible generalizations of the relevant equations for unloading, cycling loading and non-proportional loading need further experimental studies necessary to explain the nature of the specific physical phenomena involved.

Acknowledgments

This work was done within the F.U.T. Program C.E.C. U.B.I. and K.B.N. Grant 5 T07E 02825.

References

1. M. BASISTA, *Micromechanical and lattice modeling of brittle damage*, IFTR Reports, 3/2001, Warsaw 2001.
2. J. BETTEN, *Damage tensors in continuum mechanics*, J. Méch. Théor. Appl., **2**, 1, 13–32, 1983.
3. J. BETTEN, *Anwendungen von Tensorfunktionen in der Kontinuumsmechanik anisotroper Materialien*, Z. Angew. Math. Mech., **78**, 8, 507–521, 1998.
4. J.P. BOEHLER, *Applications of tensor functions in solid mechanics*, Springer-Verlag, Wien 1987.
5. J. BOGUCKA, J. DEBIŃSKI, A. LITEWKA, A.B. MESQUITA, *Experimental verification of mathematical model for oriented damage of concrete*, Mecânica Experimental, **3**, 11–18, 1998.
6. F.C.S. CARVALHO, C.N. CHEN, J.F. LABUZ, *Measurements of effective elastic modulus and microcrack density*, Int. J. Rock. Mech. Min. Sci., **34**, Paper No. 043, 1997.
7. J.L. CHABOCHE, P.M. LESNE, J.F. MAIRE, *Continuum damage mechanics, anisotropy and damage deactivation for brittle materials like concrete and ceramic composites*, Int. J. Damage Mech., **4**, 5–22, 1995.
8. W.F. CHEN, *Plasticity of reinforced concrete*, McGraw-Hill, New York 1982.
9. N.D. CRISTESCU, U. HUNSCHE, *Time effects in rock mechanics*, John Wiley & Sons, Chichester 1998.
10. W. DERSKI, R. IZBICKI, I. KISIEL, Z. MRÓZ, *Rock and soil mechanics*, Elsevier-P.W.N., Amsterdam-Warsaw 1989.

11. A. DRAGON, *On phenomenological description of rock-like materials with account for kinetics of brittle fracture*, Arch. Mech., **28**, 1, 13–30, 1976.
12. B.F. DYSON, D. MCLEAN, *Creep of Nimonic 80A in torsion and tension*, Met. Sci., **11**, 2, 37–45, 1977.
13. C. EHM, U. SCHNEIDER, *Biaxial testing of reactor concrete*, [in:] Trans. 8th Int. Conf. Structural Mechanics in Reactor Technology, North Holland, Vol. H, 349–354, Amsterdam 1985.
14. C. EIMER, *Rheological strength of concrete in the light of damage hypothesis* [in Polish], Arch. Civil Eng., **17**, 1, 15–31, 1971.
15. R.E. GOODMAN, *Introduction to rock mechanics*, John Wiley & Sons, New York 1989.
16. D. HALM, A. DRAGON, *A model of anisotropic damage by mesocrack growth; unilateral effect*, Int. J. Damage Mech., **5**, 4, 384–402, 1996.
17. D. HALM, A. DRAGON, *An anisotropic model of damage and frictional sliding for brittle materials*, Eur. J. Mech., A/Solids, **17**, 3, 439–460, 1998.
18. D.R. HAYHURST, *Creep rupture under multi-axial states of stress*, J. Mech. Phys. Solids, **20**, 381–390, 1972.
19. D.R. HAYHURST, *On the role of creep continuum damage in structural mechanics*, in: Engineering Approaches to High Temperature Design, eds. B. Wilshire, D.R.J. Owen, Pineridge Press, Swansea 1983, 85–175.
20. H. HORII, S. NEMAT-NASSER, *Overall moduli of solids with microcracks: load-induced anisotropy*, J. Mech. Phys. Solids, **31**, 2, 155–171, 1983.
21. J.W. JU, *On two-dimensional self-consistent micromechanical damage models for brittle solids*, Int. J. Solids Struct., **27**, 227–258, 1991.
22. D. KRAJCI NOVIC, *Continuum damage mechanics: when and how?*, Int. J. Damage Mech., **4**, 3, 217–229, 1995.
23. D. KRAJCI NOVIC, M. BASISTA, D. SUMARAC, *Micromechanically inspired phenomenological damage model*, J. Appl. Mech., **58**, 305–310, 1991.
24. H. KUNA-CISKAL, J. SKRZYPEK, *CDM based modeling of damage and fracture mechanisms in concrete under tension and compression*, Eng. Fracture Mech., **18**, 681–698, 2002.
25. H. KUPFER, *Das Verhalten des Betons unter mehrachsiger Kurzzeitbelastung unter besonderer Berücksichtigung der zweiachsiger Beanspruchung*, [in:] Deutscher Ausschuss für Stahlbeton, 229. Wilhelm Ernst & Sohn, 1–105, Berlin 1973.
26. F.A. LECKIE, E.T. ONAT, *Tensorial nature of damage measuring internal variables*, [in:] Physical Non-Linearities in Structures, J. HULT, J. LEMAITRE [Eds.], Springer-Verlag, 140–155, Berlin 1981.
27. J. LEMAITRE, *How to use damage mechanics*, Nucl. Eng. Design, **8**, 233–245, 1984.
28. W. LIGEZA, *Experimental stress-strain relationship for cement concrete under biaxial compression*, in: Proceedings of the International Conference Concrete and Concrete Structures, 47–54, Zilina 1999.
29. A. LITEWKA, *Effective material constants for orthotropically damaged elastic solid*, Arch. Mech., **37**, 6, 631–642, 1985.

30. A. LITEWKA, *Creep rupture of metals under multi-axial state of stress*, Arch. Mech., **41**, 1, 3-23, 1989.
31. A. LITEWKA, J. BOGUCKA, J. DĘBIŃSKI, *Deformation-induced anisotropy of concrete*, Arch. Civil Eng., **42**, 4, 425-445, 1996.
32. A. LITEWKA, J. BOGUCKA, J. DĘBIŃSKI, *Application of oriented damage theory in mechanics of concrete*, [in:] Proc. of 3rd International Conference on Analytical Models and New Concepts in Mechanics of Concrete Structures, M. KAMIŃSKI [Ed.], Oficyna Wyd. Politechniki Wrocławskiej, Wrocław 1999, 159-166.
33. A. LITEWKA, J. BOGUCKA, J. DĘBIŃSKI, *Anisotropic behaviour of damaged concrete and fibre reinforced concrete*, in: Anisotropic Behaviour of Damaged Materials, J. SKRZYPEK, A. GANCZARSKI [Eds.], Springer Verlag, 185-219, Berlin-Heidelberg 2003.
34. A. LITEWKA, J. DĘBIŃSKI, *Damage-induced anisotropy and deformability of brittle rock-like materials*, Key Eng. Materials, **230-232**, 505-508, 2002.
35. A. LITEWKA, J. DĘBIŃSKI, *Load-induced oriented damage and anisotropy of rock-like materials*, Int. J. Plast., **19**, 2171-2191, 2003.
36. A. LITEWKA, L. SZOJDA, *Tri-axial tests for brittle materials: motivation, technique, results*, Civil Env. Eng. Reports, **1**, 169-188, 2005.
37. S. MAJEWSKI, *Mechanics of structural concrete in terms of elasto-plasticity* [in Polish], Wyd. Politechniki Śląskiej, Gliwice 2003.
38. V.P. MITROFANOV, O.A. DOVZENKO, *Development of deformation induced anisotropy of concrete under uni-axial compression* [in Russian], Beton Zelezobeton, 10, 9-11, 1991.
39. S. MURAKAMI, *Progress in continuum damage mechanics*, J.S.M.E. Int. Journal, **30**, 701-710, 1987.
40. S. MURAKAMI, K. KAMIYA, *Constitutive and damage evolution equations of elastic-brittle materials based on irreversible thermodynamics*, Int. J. Mech. Sci., **39**, 4, 473-486, 1997.
41. S. MURAKAMI, N. OHNO, *A continuum theory of creep and creep damage*, [in:] Creep in Structures, A.R.S. PONTER, D.R. HAYHURST [Eds.], Springer-Verlag, 422-444, Berlin 1981.
42. A.M. NEVILLE, *Properties of concrete*, Longman, Harlow 1995.
43. E.T. ONAT, F.A. LECKIE, *Representation of mechanical behavior in the presence of changing internal structure*, J. Appl. Mech., **55**, 1-10, 1988.
44. G. PIATTI, G. BERNASCONI, F.A. COZARELLI, *Damage equations for creep rupture in steels*, Trans. 5th Int. Conf. on Structural Mechanics in Reactor Technology, North-Holland, vol. L, L11/4, 1-9, Amsterdam 1979.
45. R.S. RIVLIN, J.L. ERICSEN, *Stress-deformation relations for isotropic materials*, J. Rat. Mech. Anal., **4**, 323-425, 1955.
46. F. RUMMEL, *Brittle fracture of rocks*, [in:] Rock mechanics, L. MÜLLER [Ed.], Springer-Verlag, 85-94, Wien 1972.
47. A.J.M. SPENCER, *Theory of invariants*, [in:] Continuum Physics, C. ERINGEN [Ed.], Academic Press, vol. 1, 239-353, New York 1971.
48. L. SZOJDA, S. MAJEWSKI, *Numerical simulation of complex stress-state in masonry structure*, Proceedings of the Sixth International Masonry Conference, 471-476, London 2002.

49. K.-CH. THIENEL, F.S. ROSTASY, G. BECKER, *Strength and deformation of sealed HTR-concrete under bi-axial stress at elevated temperature*, Trans. 11th Int. Conf. on Structural Mechanics in Reactor Technology, Atomic Energy Society of Japan, vol. H, 73–78, Tokyo 1991.
50. A.A. VAKULENKO, M.L. KACHANOV, *Continuum theory of medium with cracks* [in Russian], Izv. A.N. S.S.S.R. M.T.T., 4, 159–166, 1971.

Received January 22, 2005; revised version May 16, 2005.
